Feature category systems for 2nd order local image structure induced by natural image statistics and otherwise

Lewis D Griffin & Martin Lillholm

University College London, London WC1E 6BT, UK

ABSTRACT

We report progress on an approach (Geometric Texton Theory - GTT) that like Marr's 'primal sketch' aims to describe image structure in a way that emphasises its qualitative aspects. In both approaches, image description is by labelling points using a vocabulary of feature types, though compared to Marr we aim for a much larger feature vocabulary.

We base GTT on the Gaussian derivative (DtG) model of V1 measurement. Marr's primal sketch was based on DtG filters of derivative order up to 2^{nd}, for GTT we plan to extend to the physiologically plausible limit of 4^{th}. This is how we will achieve a larger feature vocabulary (we estimate 30-150) than Marr's 'edge', 'line' and 'blob'. The central requirement of GTT then is for a procedure for determining the feature vocabulary that will scale up to 4^{th} order. We have previously published feature category systems for 1-D 1^{st} order, 1-D 2^{nd} order, 2-D 1^{st} order and 2-D pure 2^{nd} order. In this paper we will present results of GTT as applied to 2-D mixed 1^{st} + 2^{nd} order features.

We will review various approaches to defining the feature vocabulary, including ones based on (i) purely geometrical considerations, and (ii) natural image statistics.

Keywords: scale space; image derivatives; hermite transform; edge detection

1. Introduction

Similar to the scheme of Marr's 'raw primal sketch' [B1], our aim is to define a system of local image feature types, and a method for labelling each local image patch as to its feature type. We proceed according to Marr's methodology where we concentrate on the computational nature of the problem, in the hope that a sufficiently general answer will throw light on how such calculations could be carried out by biological vision systems.

As a model of image measurement, upon which to base the feature type assignment, we use derivative of Gaussian filters (DtGs). Again, this is similar to Marr's approach which was based on difference-of-gaussian filters, which are approximations of DtGs. Where we depart from Marr is our belief that recent neurophysiology suggests that a DtG model of V1 should extend up to 4^{th} order (rather than Marr's 2^{nd}). This change from 2^{nd} to 4^{th} order makes a great deal of difference. Marr guessed that the six numbers used to characterize the 2^{nd} order structure of a patch would be sufficient to categorize into a small number of classes – edge, bars and blobs: we guess that the fifteen numbers of 4^{th} order structure will be sufficient for 30+ feature types. A much larger feature vocabulary will transform the uses that the primal sketch can be put to. In particular we expect that it will be useful with much less application of the difficult-to-implement feature-grouping processes that Marr vaguely specified for constructing the full primal sketch from the raw.

Although our ambition is for a model of 4^{th} order features, in the present work we concentrate on 2^{nd} order structure. An important caveat though is that we are only interested in methods of dealing with 2^{nd} order structure that have the potential in principle and practice to generalize to higher orders.

The plan of the paper is as follows. In section 2 we will introduce the DtG model of V1. In section 3 we shall explain how local image structure has intrinsic and extrinsic components, and that feature type should be based on the intrinsic alone. In section 4 we summarize our previous work on splitting 2nd order structure into its intrinsic and extrinsic factors, and describe the 2nd order local-image-structure solid which is the intrinsic component of 2nd order structure. The feature category problem is then – how to define a partitioning of this solid into the correct feature categories. In section 5 we describe two approaches to this problem – one based on a vector quantization strategy, and the other based on geometric understanding of 2nd order structure – and present results. In section 6 we discuss the relative success of these two approaches, and the prospects for extension to higher order.

2. Gaussian derivative filters (DtGs) as a model of V1

Through experience in computer vision and from the prompt supplied by Hubel & Weisel's electrophysiology results [B2] it is widely accepted that an initial stage in any vision system should be some system of local measurement of the structure of the incident image. Casting around for developments of the notion of 'local structure' one is led to the large body of mathematical ideas initiated by the calculus of Newton & Leibniz. However, these mathematical ideas are intimately tied to the concept of derivative, defined by the infinitesimal limit $I'(0) = \lim_{\varepsilon \to 0} \varepsilon^{-1}\left(I(\varepsilon) - I(0)\right)$, and thus inapplicable to functions, such as images, that are the result of measurement. Scale Space analysis [B3;B4;B5;B6;B7;B8;B9;B10] proposes a two-step solution to the problem of operationalizing image derivative measurement. First it defines a way of changing the inner scale (roughly the size of the smallest resolvable detail) of an image by convolution (denoted $\otimes$) of the image with Gaussian kernels. Gaussian kernels of scale $\sigma \in \mathbb{R}^+$ are defined as:

$$G_\sigma(x) := \frac{1}{\sigma\sqrt{2\pi}} e^{-\frac{x^2}{2\sigma^2}}, \quad G_\sigma(x,y) := G_\sigma(x) G_\sigma(y)$$

Because of the excellent localization of the Gaussian both in space and in frequency [B11], the rescaling operation $I_\sigma = G_\sigma \otimes I$ can be performed easily and stably even if the raw image (I) is the result of physical measurement, and so discretely sampled [B3]. The second step of the Scale Space approach to calculating image derivatives is via the property $(I_\sigma)' = G'_\sigma \otimes I$, which means that the derivative of a rescaled image can be obtained by convolving the original image with a derivative of Gaussian (DtG). DtGs are defined as follows:

$$G_\sigma^{(u)}(x) := \frac{d^u}{dx^u} G_\sigma(x), \qquad G_\sigma^{(u,v)}(x,y) := G_\sigma^{(u)}(x)\, G_\sigma^{(v)}(y), \quad u, v \in \mathbb{Z}^+$$

Explicit equations for DtGs can be found using the following formula that expresses their form as the product of a 0th order gaussian multiplied by a Hermite polynomial (H_u) [B12]:

$$G_\sigma^{(u)}(x) := \left(\frac{-1}{\sigma\sqrt{2}}\right)^u H_u\left(\frac{x}{\sigma\sqrt{2}}\right) G_\sigma(x)$$

The Scale Space approach thus allows the computation of image derivatives of any order at any scale. If derivatives across the entire image are required the convolution formalism should be used; if derivatives are required at a single location only, then an inner product formalism ($\langle \_ | \_ \rangle$) is more convenient. For instance, we define image derivatives of scale σ , at the origin to be:

$$c_{uv} := (-1)^{u+v} \left\langle G_\sigma^{(u,v)} \middle| I \right\rangle := (-1)^{u+v} \int_{x,y \in \mathbb{R}} G_\sigma^{(u,v)}(x,y)\, I(x,y)$$

Note that the derivative measurements c_{uv} are dependent on the measurement scale σ , though to prevent cluttered equations we do not indicate this with a superscript. The inner-product formulation shows the similarity between the DtG approach and the operation of the simple cell neurons of area V1 of the mammalian cerebral cortex [B13]. To avoid any incorrect presumptions, we note that the DtGs are not an orthonormal set; for example $\left\langle G_\sigma^{(2,0)} \middle| G_\sigma^{(0,2)} \right\rangle = \left(16\pi\sigma^6\right)^{-1}$.

In this paper we are concerned with structure up to 2nd order, the measurement of which requires a total of six DtG filters (figure 1). The vector of derivative measurements is referred to as a jet [B14;B15], and we will later make use the perspective that regards such jets as being points in a jet space [B16;B17;B18]. Formally, the 2nd order jet at the origin is given by $\vec{j} := \begin{pmatrix} c_{00} & c_{10} & c_{01} & c_{20} & c_{11} & c_{02} \end{pmatrix}^{\mathrm{T}}$.

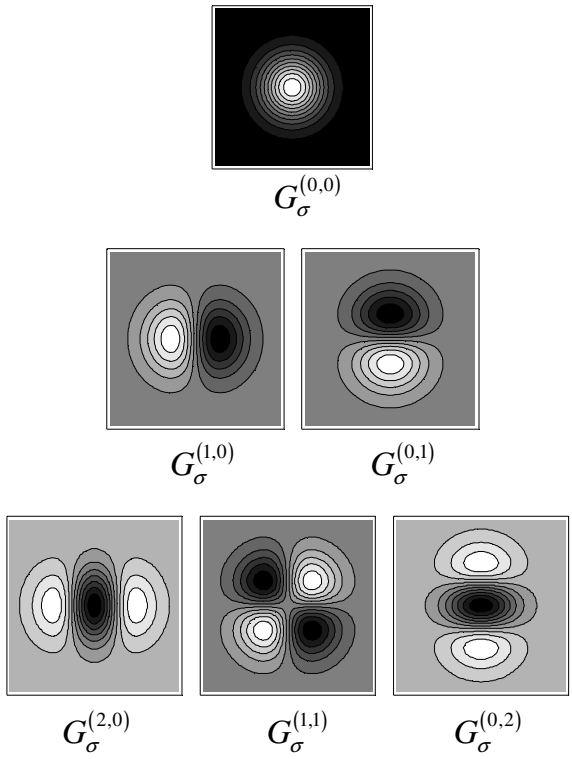

FIGURE 1 – Derivatives of the 2-D Gaussian kernel. Top row = zeroth order; middle row = 1st order; bottom row = 2nd order.

3. Intrinsic and Extrinsic local image structure

The incident image is altered by almost anything that we change about the imaging set-up, but not all changes are of equal status. In particular there are some changes (extrinsic) that we can make that change the image and yet do not change the scene that we are attempting to perceive; whilst other changes (e.g. adding an object to the scene, or a face blushing) are intrinsic. A key constraint on our method of local image description is that it should, so far as is possible, be factored into intrinsic and extrinsic components, with the property that the intrinsic component should be unaltered by extrinsic changes. In particular, we identify the intrinsic component of image description with the attachment of a feature label, the remaining aspects of image structure forming the extrinsic component.

To proceed with this approach we need to choose a list of extrinsic transformations; the following are considered in this work:

- translation of the image (NB this is dealt with by having a family of DtG filters at each location so will not be considered further),
- rotation of the image,
- reflection of the image,
- addition of a constant intensity,
- multiplication of intensities by a positive factor

We note that this list is open to debate. One can argue for additional entries (e.g. additional of luminance gradients [B19]), or removal of entries (e.g. addition of a constant intensity [B20]).

4. The 2nd order local-image-structure solid

Applying the group of extrinsic transformations moves points in jet space. Starting with a single jet, applying all possible transformations sweeps out a subspace of jet space known as an orbit. Because of the group structure of the transformations, the orbits are non-intersecting and fill jet space. In theory, one can establish a new space, each point of which corresponds to a single orbit in the jet space, and with topology induced by the adjacency of orbits. Such a space of orbits is known as an orbifold, and has a form which is manifold-like except at a limited number of locations. Below, we sketch out how we have done this.

4.1 The Orbifold topology

All components of the jet are affected by the extrinsic transformations. So, our first step is define a re-parameterization of jet space that brings this under control. We will write $\vec{k} = \begin{pmatrix} z & n & \theta & m & l & b & a \end{pmatrix}^{\mathrm{T}}$ for a vector composed of the new parameters, and $\Omega = \mathbb{R} \times \mathbb{R}^{+} \times (-\pi, \pi] \times \{-1, 1\} \times [-\pi/2, \pi/2] \times [0, \pi/2] \times [0, \pi/2]$ for the domain of $\vec{k}$. The mapping ($\vec{r}$) from the derivative representation $\vec{j}$ to the re-parameterization is given by:

$$\vec{k} = \begin{pmatrix} z \\ n \\ \theta \\ m \\ l \\ b \\ a \end{pmatrix} = \vec{r}\left(\vec{j}\right) = \begin{pmatrix} c_{00} \\ \left\|\vec{j}\right\| \\ \tan^{-1} c_{01}/c_{10} \\ \operatorname{sgn}^{+}\left(\tan^{-1}\left(2\dfrac{\left(c_{01}^2 - c_{10}^2\right)c_{11} + c_{10}\,c_{01}\left(c_{20} - c_{02}\right)}{\left(c_{01}^2 - c_{10}^2\right)\left(c_{02} - c_{20}\right) + 4c_{10}\,c_{01}\,c_{11}} \right) \right) \\ \tan^{-1}\left(\dfrac{\sigma\left(c_{20} + c_{02}\right)}{\sqrt{4\left(c_{10}^2 + c_{01}^2\right) + \sigma^2\left(\left(c_{20} - c_{02}\right)^2 + 4c_{11}^2\right)}} \right) \\ \tan^{-1}\left(\sigma\sqrt{\dfrac{\left(c_{20} - c_{02}\right)^2 + 4c_{11}^2}{4\left(c_{10}^2 + c_{01}^2\right)}} \right) \\ \tfrac{1}{2}\left| \tan^{-1}\left(2\dfrac{\left(c_{01}^2 - c_{10}^2\right)c_{11} + c_{10}\,c_{01}\left(c_{20} - c_{02}\right)}{\left(c_{01}^2 - c_{10}^2\right)\left(c_{02} - c_{20}\right) + 4c_{10}\,c_{01}\,c_{11}} \right) \right| \end{pmatrix}$$

It can be confirmed that amongst the new parameters, only *l*, *b* and *a* are unaffected by all the extrinsic transformations. These three parameters are thus a coordinate system for the orbifold [B21] which we seek to define. Although the domains of *l*, *b* and *a* are the open intervals $\left[-\tfrac{\pi}{2}, \tfrac{\pi}{2}\right]$, $\left[0, \tfrac{\pi}{2}\right]$ and $\left[0, \tfrac{\pi}{2}\right]$ respectively, the topology of the orbifold is not that of a cuboid. For example, when $|l| = \tfrac{\pi}{2}$ it can be seen that the values of *b* and *a* are irrelevant. Continuing this style of

analysis, one concludes that the topology is as follows. Start with a cuboid. Squash the left and right faces of the cuboid each into a vertical line. Squash the top and bottom faces of the cuboid into points.

4.2 The Orbifold metric

As per the standard definition, the orbifold that we have defined is a manifold except on its boundary, but is not yet equipped with a metric. To supply a metric, we argue for a particular norm on the jet space, use the norm to define a metric on jet space, and use this to induce a metric on the orbifold. The jet space norm that we argue for elsewhere [B22] is the Gaussian-windowed standard deviation of the function that (i) measures to the jet, and (ii) minimizes the Gaussian-windowed standard deviation. In turns out that the unique function that satisfies these requirements is the unique polynomial (of the same order as the jet) that measures to the jet. This has been named the jet space polynomial. The 2nd order jet space polynomial is:

$$P_{\vec{j}}(x,y) \coloneqq \left(c_{00} - \tfrac{1}{2}\sigma^2\left(c_{20}+c_{02}\right)\right) + \left(c_{10}\,x + c_{01}\,y\right) + \tfrac{1}{2}\left(c_{20}\,x^2 + 2c_{11}\,x\,y + c_{02}\,y^2\right)$$

and its Gaussian-windowed standard deviation, and hence (by definition) the jet norm is:

$$\left\|\vec{j}\right\| \coloneqq \left(\sigma^2\left(c_{10}^2 + c_{01}^2\right) + \tfrac{1}{2}\sigma^4\left(c_{20}^2 + 2c_{11}^2 + c_{02}^2\right)\right)^{\frac{1}{2}}$$

The jet space metric is induced in the normal way:

$$d\left(\vec{p},\vec{q}\right) \coloneqq \left\|\vec{p}-\vec{q}\right\|$$

We use the jet space metric to induce a metric on the orbifold as follows. For each of two points in the orbifold, consider the sets of unit norm jets that map to those points. Find the shortest path of unit norm jets that link the two sets of jets. Measure the length of the linking path using the jet space metric. The result is the orbifold metric distance between the two orbifold points.

We are only able to carry out the calculation above for orbifold point pairs that are infinitesimally close. This has allowed us to determine the metric tensor of the orbifold (written as a line element, $ds^2 = dl^2 + \cos^2 l\left(db^2 + \frac{2\sin^2 2b}{5-3\cos 2b}da^2\right)$) but we are not able (as of yet) to compute metric distances between arbitrary points except by difficult numerical integration methods.

4.2 The Orbifold embedding

From the metric tensor one can calculate that the scalar curvature of the orbifold is $\kappa_{scalar} = 6 + \frac{96\sec^2 l}{\left(5-3\cos 2b\right)^2}$. This shows that the intrinsic curvature is non-constant, and so the orbifold does not have the intrinsic geometry of some region of Euclidean 3-space. This is inconvenient as it prevents the simplest approaches to visualizing its shape. Instead, we are forced to find an embedding [B23] of the orbifold into Euclidean 3-space. Fortunately, since the $\langle l, b, a\rangle$ coordinate system led to a diagonal metric tensor, finding an embedding is not difficult. In particular:

$$\vec{\chi}\left(\begin{pmatrix} l \\ b \\ a \end{pmatrix}\right) = \begin{pmatrix} \left(b-\frac{\pi}{4}\right)\cos l \\ \left(a-\frac{\pi}{4}\right)\sqrt{2}\,\frac{\cos l \sin 2b}{\sqrt{5-3\cos 2b}} \\ -l \end{pmatrix}_{xyz}$$

The embedding is certainly not isometric but it has been constructed so that it preserves intrinsic volumes (demonstrated elsewhere [B22]). The degree of the failure of isometry can be quantified by saying that the infinitesimal spheres in the orbifold get embedded as ellipsoids with a median eccentricity of 1.30, and a mean of 1.46 – where eccentricity is largest

diameter divided by smallest. The embedded orbifold is shown in figure 2, where it can be seen that it is shaped something like a lemon, partially flattened normal to its axis of symmetry. We refer to it as the 2nd-order local-image-structure solid.

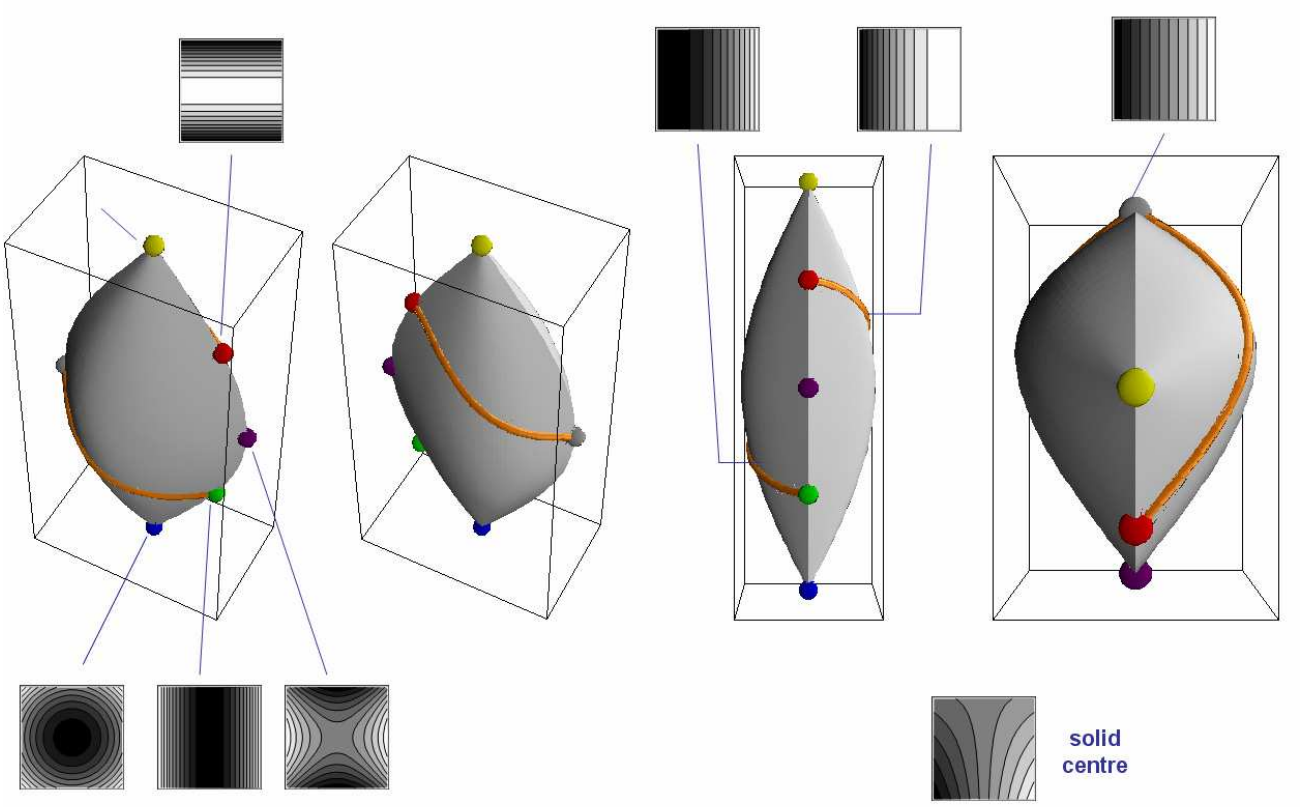

FIGURE 2 – The 2nd-order local-image-structure solid, which is the embedding of the orbifold into $\mathbb{R}^3$ using the mapping $\vec{\chi}$. The four surface-rendered panels show different views of the solid. The density plots show examples of local structure, with the connectors showing where they map to in the solid; the local structure at bottom-right, without a connector, corresponds to the centre of the solid. The shape of the solid is roughly that of a lemon, flattened perpendicular to the main axis of symmetry to produce two sharp edges. Notice though that the two sharp edges are not the same shape (rightmost view). The sharp vertices of the solid at its top and bottom correspond to umbilic points. The sharp edge with five special points marked on it is the locus of local forms that have vanishing 1st order structure. The locus runs from the maximum umbilic point (blue) at top, through to a ridge shape (green), a balanced saddle [B24;B25] (purple), a rut (green), to the minimum umbilic point (blue) at bottom. The grey point on the other sharp edge corresponds to vanishing 2nd order structure. The orange arcs, which travel over the smooth faces of the solid, marks local structure which is effectively 1-D. The arc is on the surface of the solid, because the surface corresponds to local structure where the angular 1st and 2nd order components of the local structure are at 0° or 90°, which is a necessary condition for local structure to be 1-D.

5. Defining feature categories

In Griffin & Lillholm ([B18]) we made explicit three hypotheses about image features, and grouped them under the banner ‘geometric texton theory’. The first hypothesis was:

> the *Feature Hypothesis*: that there exists a system of qualitative description of local structure that is (i) based on a partitioning of jet space into feature categories, and (ii) is useful for subsequent stages of processing.

We have since refined this hypothesis to say that it is the intrinsic factor of jet space that should be partitioned.

The second and third hypotheses concerned what determined the partitioning. These hypotheses were predicated on the view that metamerism was a key concept. Metamerism in this context referring to the fact that there is an effectively infinite collection of images (the metamery class) that could explain any given jet measurement. The second hypothesis concerned the role of iconic exemplars from the metamery class:

> the *Icon Hypothesis*: that (i) each metamery class contains an iconic representative, and (ii) the equivalence relation of qualitative similarity of icons is what determines the partitioning of the Feature Hypothesis.

The third hypothesis concerned what determined the iconic exemplars:

> the *Texton Hypothesis:* that the icons of the Icon Hypothesis are the elements of metamery classes that are the most common in natural images.

We have pursued these hypotheses and produced good results for the 1-D 1st order [B26] and 2nd order jets [B27]. Unfortunately we have found that applying our method to the 2-D case, that in which we are truly interested, is computationally very difficult because of the amount of data needed to perform the high-dimensional mode estimation required. Without retracting the icon and texton hypotheses, in this work we depart from them – we keep the feature hypothesis (or rather the refine version of it) but examine two, more tractable, approaches to defining categories.

5.1 A geometric approach

Categorization has been studied for a long time using philosophical/theoretical and experimental methods. A wide variety of specific domains (e.g. colours, animals) have been considered, as has the abstract case [B28;B29;B30;B31;B32;B33;B34;B35;B36;B37]. Historically, the earlier conception of categories being induced by membership-defining properties has been superseded by the idea that categories are induced by a system of prototypes (one or more per category) plus the rule that elements belong to the category whose prototype they are most similar to [B38].

We have applied this prototype approach to the problem of partitioning the 2nd order solid. To prevent confusion at the outset, we stress that icons and prototypes should not be confused. A different icon, in the sense introduced at the beginning of section 5, is associated with each point of jet space; whereas prototypes are particular points of jet space. To apply the prototype approach to our problem we must follow the following steps: (i) identify a system of special locations in the 2nd order solid, (ii) construct the voronoi partitioning induced by the special locations using the orbifold metric.

For our special locations in the solid, we use the six points marked in figure 2. These six points consist of the pure 1st order point and five pure 2nd order points. The pure 2nd order points are equally-spaced (according to the orbifold metric) along the pure 2nd order locus and correspond to the maximal and minimal umbilic points, the convex and concave parabolic points and the balanced saddle point. At this stage we offer no defining characterisation of these special locations such as will allow us to generalize to higher orders, but report that an approach that considers the spatial symmetries of the jet space polynomials is promising.

The next step in following this program of category definition is to construct voronoi cells about our selected prototype locations. At this stage all we can offer is a guess, shown in figure 3, at these cells. We will refer to them as 'voronoi' cells. Using the embedding we have confirmed that the 'voronoi' cells are at least approximately voronoi, but more work needs to be done on this. The 'voronoi' cells are bounded by iso-surfaces of differential invariants. The curving boundary that defines the category around the pure 1st order prototype is a surface of constant ratio between the 1st and 2nd order components of the norm. In terms of the *lba*-coordinate system for the solid, the surface is given by $\sec l \sec b = \sqrt{2}$. The four triangular boundaries are parts of surfaces of constant shape index. Shape index (ι) is a pure second order differential invariant that measures the ratio between the principal curvatures of the image [B39]. The surfaces are determined using the following relation with our solid coordinate system $\tan \iota = \csc b \tan l$. Only the portions of the surfaces where $\sec l \sec b \geq \sqrt{2}$ are used so that they do not protrude into the pure 1st order category.

Also shown in figure 3 are the categories as solid lumps of the solid (for comparison with the results in section 5.4) and the feature labels computed for an example natural image. These will be discussed in the final section.

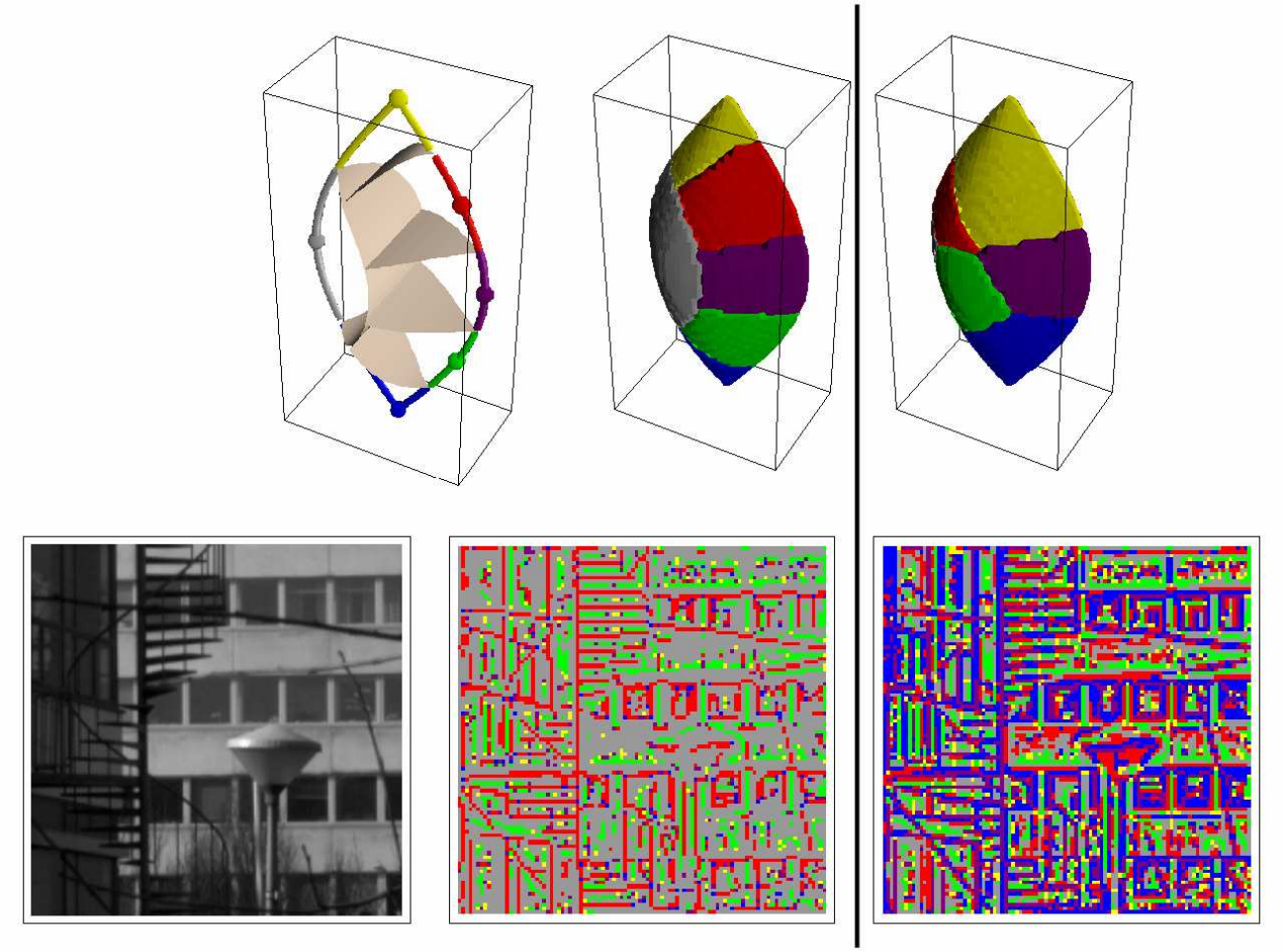

FIGURE 3 – Category structures on the 2nd order solid. Left of the vertical line shows results for section 5.3, right for section 5.4. At top left are shown the system of 'voronoi' boundaries that we have defined to separate the exceptional points of the solid. Top middle shows the category system at left as a set of solid sub-volumes. Top right shows the category system that we derived through a rate-distortion minimization approach – the colours used have been chosen so that they agree with those used in the constructed system as far as is possible. Along the bottom is shown an example natural image and the feature categories according to the schemes shown above them. The derivatives for the feature classification scheme were calculated at a scale of $\sigma = 1.4$ and the feature labels are shown with a pixel size of 2.0.

5.4 A Quantization approach

There is a mature body of literature on the problem of optimally quantizing a vector or a scalar variable [B40]. Optimality is assessed with respect to two measures. One, *variance-accounted-for*, captures how much of the source variable is encoded by the quantized variable; the other, *rate*, looks at the entropy cost of coding the quantized variable. One may, for example seek for the quantization strategy that accounts for the most variance while using a code that takes (say) no more than 5.3 bits optimally to encode.

As an experiment in this approach we have computed the optimal quantization of the structure solid into six (for comparison with 5.3) categories – where optimality is defined as accounting-for-variance. For this computation we made

use of a histogram of the rates of different types of intrinsic 2nd order structure that occurs in natural images that we have computed previously. This histogram is illustrated in figure 4, where it can be seen to be non-trivial in neither being uniform nor being the same as pink noise (i.e. noise with a 1/f fourier amplitude spectrum like natural images, and random phases).

We computed the optimal quantization using simulated annealing. Variances were calculated using distances in the embedding as an approximation of geodesic distances. Performing many runs of the algorithm has convinced us that we have achieved a near optimal quantization, but shown us that there are multiple competing near-optimal quantizations. The best quantization we found is shown in figure 3. It accounts for 73% of the variance. Since the categories it has found contain near equal amounts of the natural image distribution, the entropy cost of coding the categories (2.52 bits) is near the maximum $\log_2 6 \approx 2.58$. In comparison, the prototype-based categories account for only 56% of the variance, but require only 1.61 bits to encode. In terms of efficiency, the quantization approach accounts for 29% of the variance per bit of encoding, while the prototype approach accounts for 35% per bit.

Figure 3 also shows the quantization based categories used to feature label an example grey-level image. This will be discussed in the next section.

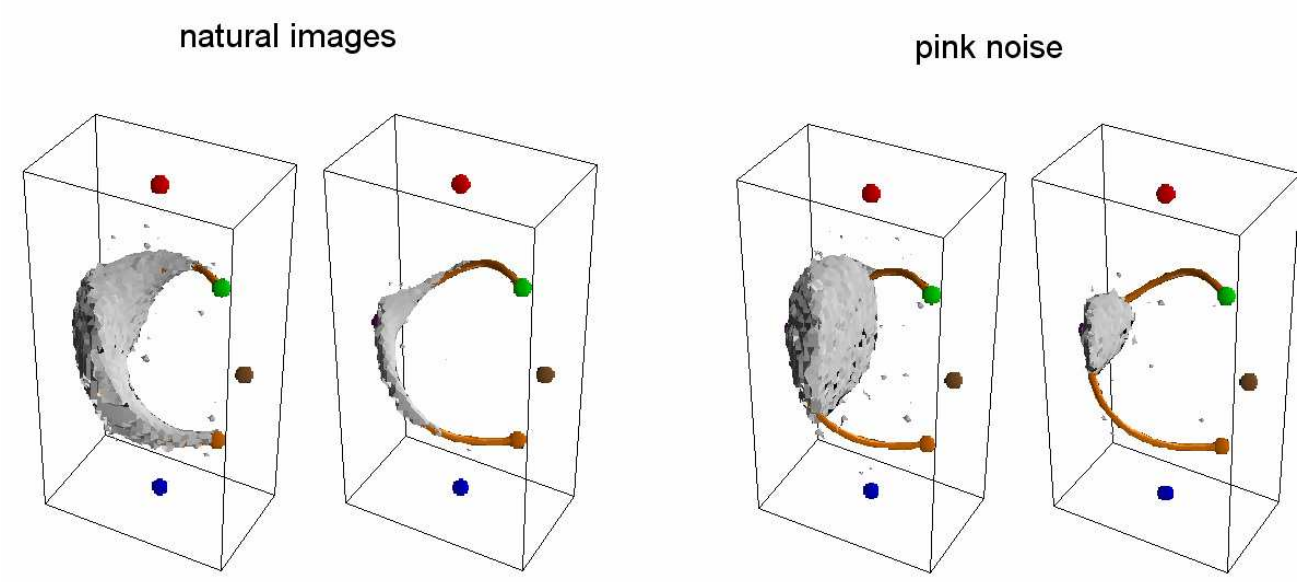

FIGURE 4 - The figure shows iso-density contours of the histogram of local forms for natural images and pink noise. The left panel of each pair shows the iso-density surface that surrounds 50% of the total histogram density; the right panels 10% of the density. For orientation, the same special points and curves are shown as in figure 2. It can be seen that natural images shown an excess of locally 1-D structure compared to pink noise.

6. Discussion

The aim of this work was to try two approaches to the problem of partitioning factored jet spaces into feature categories, and to assess them for effectiveness and ease of generalization to higher dimensions. For effectiveness, we can consider the measures of quantization theory as given in the previous section. The results are equivocal. The variance-based approach successfully accounts for more variance than the geometric approach, but does so with a slightly more expensive code. We can also consider how the features look on example images such as shown in figure 3. Again the results are equivocal. The quantization-based features are 'busier', but that is to be expected given the more expensive code. Does one set of features capture the qualitative image structure better than the other? We invite the reader to judge for themselves, but for ourselves we feel that we cannot answer with confidence. What is needed of course is an

objective measure of 'capturing qualitative structure', but if we *had* such a measure with certainty we could use it to find the optimal categories so the puzzle would not present itself.

Acknowledgements

Research undertaken as part of EPSRC-funded project 'Basic Image Features'.

References

[B1] Marr, D., *Vision* New York: W H Freeman & co, 1982.

[B2] Hubel, D. H. and Wiesel, T. N., "Receptive fields and functional architecture of monkey striate cortex," *Journal of Physiology*, vol. 195 pp. 215-243, 1968.

[B3] Koenderink, J. J., "The Structure of Images," *Biological Cybernetics*, vol. 50, no. 5, pp. 363-370, 1984.

[B4] Scale-Space Theory in Computer Vision. ter Haar Romeny, B. M. LNCS vol. 1252. 1997. Springer-Verlag.
Ref Type: Conference Proceeding

[B5] Scale-Space and Morphology in Computer Vision. Kerckhove, M. LNCS vol. 2106. 2001. Springer-Verlag.
Ref Type: Conference Proceeding

[B6] Scale Space and PDE methods in Computer Vision. Kimmel, R., Sochen, N., and Weickert, J. LNCS vol. 3459. 2006. Springer-Verlag.
Ref Type: Conference Proceeding

[B7] Scale-Space theories in Computer Vision. Nielsen, M. LNCS vol. 1682. 1999. Springer-Verlag.
Ref Type: Conference Proceeding

[B8] Scale Space methods in Computer Vision. Griffin, L. D. and Lillholm, M. LNCS vol. 2695. 2003. Springer-Verlag.
Ref Type: Conference Proceeding

[B9] Lindeberg, T., *Scale-Space Theory in Computer Vision* Kluwer Academic Publishers, 1994.

[B10] Florack, L. M. J., *Image Structure* Springer, 1997.

[B11] Victor, J. D. and Knight, B. W., "Simultaneously band and space limited functions in two dimensions, and receptive fields of visual neurons," in Kaplan, E., Marsden, J., and Sreenivasan, K. (eds.) *Perspectives and Problems in Nonlinear Science* Springer-Verlag, 2002, pp. 370-420.

[B12] Abramowitz, M. and Stegun, I. A., *Handbook of Mathematical Functions* New York: Dover Publications, 1964.

[B13] Ringach, D. L., "Spatial structure and symmetry of simple-cell receptive fields in macaque primary visual cortex," *Journal of Neurophysiology*, vol. 88 pp. 455-463, 2002.

[B14] Florack, L. M. J., ter Haar Romeny, B. M., Viergever, M. A., and Koenderink, J. J., "The gaussian scale-space paradigm and the multiscale local jet," *International Journal of Computer Vision*, vol. 18 pp. 61-75, 1996.

[B15] Lillholm, M. and Pedersen, K. S., "Jet based feature classification," *Proceedings of the 17th International Conference on Pattern Recognition, Vol 2* 2004, pp. 787-790.

[B16] Iijima, T., "A system of fundamental functions in an abstract figure space," *Systems, Computers, Controls.*, vol. 2, no. 6, pp. 96-103, 1971.

[B17] Pedersen, K. S. and Lee, A. B., "Toward a full probability model of edges in natural images," *Computer Vison - Eccv 2002, Pt 1* 2002, pp. 328-342.

[B18] Griffin, L. D. and Lillholm, M., "Hypotheses for image features, icons and textons," *International Journal of Computer Vision*, 32767.

[B19] Koenderink, J. J. and van Doorn, A. J. Image processing done right. Heyden, A., Sparr, G., Nielsen, M., and Johansen, P. 2350, 158-172. 2002. Copenhagen, Springer. LNCS.
Ref Type: Conference Proceeding

[B20] Harley, E. M., Dillon, A. M., and Loftus, G. R., "Why is it difficult to see in the fog? How stimulus contrast affects visual perception and visual memory," *Psychonomic Bulletin & Review*, vol. 11, no. 2, pp. 197-231, 2004.

[B21] Thurston, W. P., *The Geometry and Topology of Three-Manifolds*, Electronic Version 1.1 ed. Mathematical Sciences Research Institute, 2002.

[B22] Griffin, L. D., "The 2nd order local-image-structure solid," *IEEE Transactions on Pattern Analysis and Machine Intelligence*, 2007.
[B23] Doran, C. and Lasenby, A., *Geometric Algebra for Physicists* Cambridge: Cambridge University Press, 2003.
[B24] Griffin, L. D. and Colchester, A. C. F., "Superficial and Deep-Structure in Linear Diffusion Scale-Space - Isophotes, Critical-Points and Separatrices," *Image and Vision Computing*, vol. 13, no. 7, pp. 543-557, 1995.
[B25] Koenderink, J. J., "A Hitherto Unnoticed Singularity of Scale-Space," *IEEE Transactions on Pattern Analysis and Machine Intelligence*, vol. 11, no. 11, pp. 1222-1224, 1989.
[B26] Griffin, L. D., Lillholm, M., and Nielsen, M., "Natural image profiles are most likely to be step edges," *Vision Research*, vol. 44, no. 4, pp. 407-421, 2004.
[B27] Griffin, L. D., "Feature classes for 1-D, 2nd order structure arise from the maximum likelihood statistics of natural images," *Network: Computation in Neural Systems*, vol. 16, no. 2/3, pp. 301-320, 2005.
[B28] Acker, B. E., Pastore, R. E., and Hall, M. D., "Within-Category Discrimination of Musical Chords - Perceptual Magnet or Anchor," *Perception & Psychophysics*, vol. 57, no. 6, pp. 863-874, 1995.
[B29] Belpaeme, T., "Reaching coherent color categories through communication.," in Krose, B. (ed.) *Proc. 13th Belgium-Netherlands conf. on AI* 2001, pp. 41-48.
[B30] Bimler, D. and Kirkland, J., "Categorical perception of facial expressions of emotion: Evidence from multidimensional scaling," *Cognition & Emotion*, vol. 15, no. 5, pp. 633-658, 2001.
[B31] Bornstein, M. H., "Perceptual categories in vision and audition," in Harnad, S. (ed.) *Categorical Perception: The groundwork of cognition* Cambridge: Cambridge University Press, 1987.
[B32] Boynton, R. M., Fargo, L., Olson, C. X., and Smallman, H. S., "Category effects in color memory," *Color Research and Application*, vol. 14 pp. 229-234, 1989.
[B33] Campanella, S., Chrysochoos, A., and Bruyer, R., "Categorical perception of facial gender information: Behavioural evidence and the face-space metaphor," *Visual Cognition*, vol. 8, no. 2, pp. 237-262, 2001.
[B34] Davidoff, J., Davies, I., and Roberson, D., "Colour categories in a stone-age tribe," *Nature*, vol. 398, no. 6724, pp. 203-204, 1999.
[B35] Hardin, C. L., "Basic Color Terms and Basic Color Categories," in Backhaus, K. &. W. (ed.) *Color Vision: Perspectives from Different Disciplines* Berlin and New York: Walter de Gruyter, 1998.
[B36] Jameson, K. A. and Alvarado, N., "The relational correspondence between category exemplars and names," *Philosophical Psychology*, vol. 16, no. 1, pp. 25-49, 2003.
[B37] Kay, P., "Color categories are not arbitrary," *Journal of Cross-Cultural Research*, 32767.
[B38] Gärdenfors, P., *Conceptual Spaces: the geometry of thought* Cambridge MA: MIT Press, 2000.
[B39] Koenderink, J. J. and van Doorn, A. J., "Surface Shape and Curvature Scales," *Image and Vision Computing*, vol. 10, no. 8, pp. 557-565, 1992.
[B40] Sayood, K., *Introduction to Data Compression*, 3rd ed. Morgan Kaufmann Publishers Inc., 2005.